

# Deformation monitoring at shield tunnel joints: Laboratory test and discrete element simulation

Maoyi Mao<sup>1</sup>  | Xiaowei Yang<sup>1</sup> | Chun Liu<sup>1</sup> | Tao Zhao<sup>2</sup> | Hui Liu<sup>1</sup>

<sup>1</sup>School of Earth Sciences and Engineering, Nanjing University, Nanjing, China

<sup>2</sup>Department of Civil and Environmental Engineering, Brunel University London, London, UK

## Correspondence

Chun Liu, School of Earth Sciences and Engineering, Nanjing University, Nanjing 210023, China.  
Email: [chunliu@nju.edu.cn](mailto:chunliu@nju.edu.cn)

## Funding information

National Natural Science Foundation of China, Grant/Award Numbers: 41977218, 42222707; State Key Laboratory for GeoMechanics and Deep Underground Engineering, Grant/Award Number: SKLGDUEK2117

## Abstract

Shield tunnel, composed of several segments, is widely used in urban underground engineering. When the tunnel is under load, relative displacement occurs between adjacent segments. In the past, distributed optical fiber sensing technology was used to perform strain monitoring, but there is an urgent need to determine how to transform strain into displacement. In this study, optical frequency domain reflectometry was applied in laboratory tests. Aiming at the shear process and center settlement process of shield tunnel segments, two kinds of quantitative calculation methods were put forward to carry out a quantitative analysis. Meanwhile, the laboratory test process was simulated numerically utilizing the discrete element numerical analysis method. Optical fiber, an atypical geotechnical material, was innovatively applied for discrete element modeling and numerical simulation. The results show that the measured displacement of the dial gauge, the calculated results of the numerical model, and the displacement quantitatively calculated from the optical fiber data agree with each other in general. The latter two methods can potentially be utilized in engineering application of deformation monitoring at shield tunnel joints, but need to be further calibrated and adjusted in detail.

## KEYWORDS

discrete element method, distributed optical fiber, MatDEM, OFDR, shield tunnel

## Highlights

- The optical frequency domain reflectometry technology is applied in the monitoring of dislocation of tunnel segments in the laboratory.
- Two original calculation methods are proposed to quantify the deformation between adjacent tunnel segments, and to quantitatively monitor the displacement of shield tunnel segments under load.
- A discrete element model is developed, and two kinds of deformation processes are simulated using an innovative high-performance discrete element software, MatDEM, developed by our group.

## 1 | INTRODUCTION

Subways are an important part of urban rail transit. In recent years, subways have been built on a large scale to solve the problem of urban traffic congestion. Shield tunnel, as the main carrier of urban subways, has been widely used in major cities in China. During the construction of a shield tunnel, the soil around the tunnel is affected by additional stress due to the influence of foundation pit excavation, ground loading and unloading, and changes in geological conditions (Katebi et al., 2015; Koyama, 2003; Li et al., 2021; Nomoto et al., 1999).

Additionally, with increasing use, the tunnel will undergo deformation and damage to different degrees due to the long-term action of additional stresses (Guan et al., 2020; Jallow et al., 2019; Wang et al., 2019). Therefore, long-term monitoring and numerical analysis of the condition of the tunnel are essential.

Shield tunnels are composed of a series of tunnel segments, and there exists a certain gap between two adjacent segments. When the pipeline is subjected to load, the gap will close or open unevenly. Furthermore, dislocation of adjacent shield tunnels may occur during engineering activities, such as excavation of the foundation

This is an open access article under the terms of the [Creative Commons Attribution](https://creativecommons.org/licenses/by/4.0/) License, which permits use, distribution and reproduction in any medium, provided the original work is properly cited.

© 2024 The Authors. *Deep Underground Science and Engineering* published by John Wiley & Sons Australia, Ltd on behalf of China University of Mining and Technology.

pit (Caratelli et al., 2011). Researchers have conducted many studies to explore the correlation of external deformation and shield tunnel deformation. They proposed early warning measures for ground collapse and structural damage (Kavvas, 2005; Kawakami, 1984; Wei et al., 2018). Traditionally, several strain gauges and water-pressure gauges were mounted on tunnel rings in order to gain detailed insight into the strain and stress distribution around the tunnel, but the monitoring was inconsistent (Bakker et al., 1999; Hashimoto et al., 2008). Nowadays, with the development of sensor technology, the image sensor network along with the deep learning technique is utilized to monitor the vertical settlement caused by internal and external stresses after the subway tunnel has been in use for a long time, so as to provide early warning measures for tunnel deformation (Huang et al., 2018; Sun et al., 2020; Xiong et al., 2010; Zhao et al., 2020).

Besides the monitoring methods mentioned above, the distributed optical fiber sensing technology has been widely used in the process of longitudinal and horizontal displacement monitoring in the last decade, due to its high sensitivity, convenience in terms of setup, distributed measurement, and long service life (Fajkus et al., 2017; Gómez et al., 2020; Mohamad et al., 2012). Distributed fiber optic sensing (DFOS) systems based on Brillouin optical time domain reflectometry, Brillouin optical frequency domain analysis, and so on are utilized to monitor the stress and strain development of shield tunnels combined or not combined with traditional monitoring methods such as total stations (Gue et al., 2015; Monsberger & Lienhart, 2021). Moreover, field monitoring is usually combined with numerical simulations to investigate the mechanism of deformation of shield tunnels. Both the finite element method and the discrete element method (DEM) are used to study the tunnel deformation characteristics and tunnel failure mechanism (Juárez-Luna & Tenorio-Montero, 2019; Lee & Bassett, 2006; Moussaie et al., 2019).

Although DFOS has been successfully applied in the distributed strain monitoring of shield tunnels, because the optical fiber can only directly monitor the longitudinal strain, there still remains a critical difficulty in detecting the relative dislocation of adjacent tunnel segments, such as relative rotation and shear displacement of tunnels, which is generally the focus of field monitoring (Cheng & Ni, 2009; Wang et al., 2018; Zhang & Broere, 2023). In this study, the optical frequency domain reflectometry (OFDR) technology was applied for monitoring of dislocation of tunnel segments in the laboratory. Two calculation methods were proposed to quantify the deformation between adjacent tunnel segments, and to quantitatively monitor the displacement of shield tunnel segments under load. Based on the high-performance discrete element software, MatDEM, a discrete element model of tunnel was developed, and two kinds of deformation processes were simulated. The laboratory test results were compared with the optical fiber monitoring results, and the physical test process was reproduced on a computer by numerical simulation.

## 2 | METHODS AND PRINCIPLES

### 2.1 | Technical principles of OFDR

When light passes through an uneven medium, it undergoes deviation in the direction in which it is traveling. This is called light scattering. The scattering of light can be divided into Rayleigh scattering, Brillouin scattering, and Raman scattering. In Rayleigh scattering, the wavelength and frequency of incident light do not change after scattering, so it is also called elastic scattering. In Brillouin scattering and Raman scattering, due to the effect of the acoustic wave field in the light, scattered light will be generated with a higher or lower frequency than the frequency of the original incident light. This is called inelastic scattering. The OFDR is a back-reflection technique based on Rayleigh scattering, whose technical principle is shown in Figure 1. When the light from the source passes through the coupler, it is divided into signal light and reference light. The signal light and the reference light pass through the coupler to the photodetector for coherent mixing. When the sensing fiber is affected by the temperature field or the strain field at different positions, the refractive index of the fiber at that position will change. This will cause a change in the signal light frequency, and the frequency difference between the signal light and the reference light will change accordingly.

The OFDR technology can be used to monitor the strain along the fiber by means of coherence detection of a sweep light source. Coherence detection is an indirect detection technique that converts a high-frequency optical signal into a medium-frequency optical signal. This technology is not limited by pulse width and dynamic range, and has a large dynamic range as well as a high spatial resolution (Ma et al., 2019). The spatial resolution of OFDR can reach up to 1 mm.

### 2.2 | DEM

A linear elastic contact model of the DEM is adopted in the numerical simulation. As shown in Figure 2, two elements interact with each other through a breakable spring. The normal and tangential springs control the normal and tangential distances of the adjacent elements, respectively (Liu et al., 2013). The force is generated at the point of contact between adjacent particle elements. The normal force between adjacent particles is the product of the normal stiffness and the relative displacement:

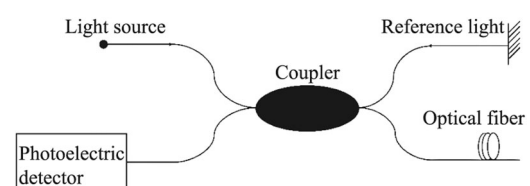


**FIGURE 1** Technical principle of optical frequency domain reflectometry.

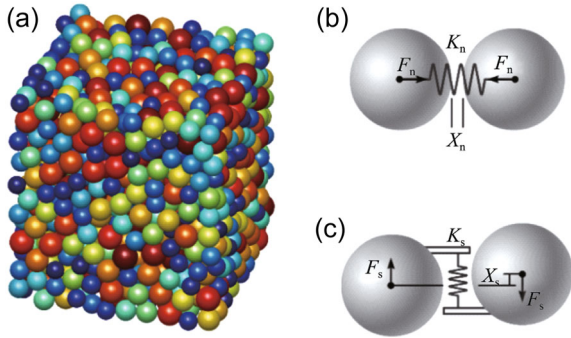


**FIGURE 2** (a) A 3D stacking model. (b, c) Normal and tangential springs between the elements.

$$\text{Intact connection: } F_n = K_n \times X_n \quad (X_n < X_b), \quad (1)$$

$$\text{Broken connection: } \begin{cases} F_n = K_n \times X_n & (X_n < 0), \\ F_n = 0 & (X_n > 0), \end{cases} \quad (2)$$

where  $F_n$  denotes the normal force;  $K_n$  denotes the normal stiffness;  $X_n$  is the normal relative displacement; and  $X_b$  is the breaking displacement. The elements interact with each other by the spring force (Equation 1) until the normal displacement ( $X_n$ ) exceeds the breaking displacement ( $X_b$ ), the connection between particles is broken, and only compressive force exists between adjacent elements (Equation 2). Similarly, the intact tangential force can be calculated using the following formula:

$$F_s = K_s \times X_s, \quad (3)$$

where  $K_s$  denotes the shear stiffness and  $X_s$  is the shear relative displacement.

The spring also has a failure criterion in the tangential direction, which is based on the Mohr–Coulomb criterion:

$$F_{s\max} = F_{s0} - \mu_p \times F_n, \quad (4)$$

where  $F_{s\max}$  denotes the maximum shear force;  $F_{s0}$  is the inter-element initial shear resistance; and  $\mu_p$  is the inter-element coefficient of friction. In the Mohr–Coulomb criterion, the maximum shear resistance between elements is related to the initial shear resistance ( $F_{s0}$ ).  $F_{s0}$  represents the maximum shear force allowed between elements without applying normal pressure. It can be analogized to the cohesion found in rock and soil mass. The normal stress is positively correlated with the shear resistance. When the magnitude of the shear force exceeds the maximum shear force, the tangential connection is broken, and only the sliding friction force ( $-\mu_p * F_n$ ) acts between the elements.

## 2.3 | Elastic clump model

In order to build tunnel segments with a relatively smooth surface, a new elastic clump model is proposed. For instance, as shown in Figure 3, the two elements of diameter  $d$  overlap with a length  $l_0$ , so the original equilibrium distance between these two elements is

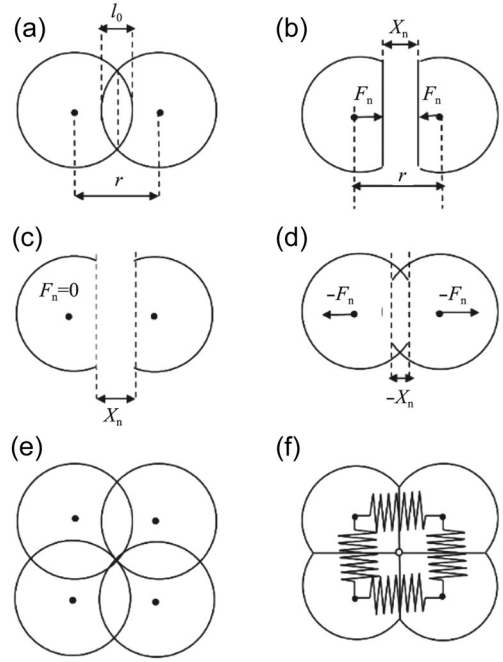


**FIGURE 3** Elastic clump calculation principle. (a) Elements in a state of equilibrium; (b) elements in a tensile state; (c) elements after the connection breaks; (d) elements in (c) are compressed again; and (e, f) four elements overlap with each other.

( $d - l_0$ ). The distance between the two elements is shown by  $r$ ; thus, the relative displacement between the elements can then be calculated as:

$$X_n = r - (d - l_0). \quad (5)$$

According to this equation, in the state shown in Figure 3a, the relative displacement  $X_n$  of the two elements is zero and they are in a state of equilibrium. In Figure 3a, the vertical line segment is the contact surface of the two elements. In Figure 3b, when the distance between the two elements increases,  $X_n$  increases and tension is generated between these two elements.

As in the real world, when the relative displacement reaches the fracture displacement  $X_b$ , the connection breaks (Figure 3c) and is followed by cementing again. When the two elements are compressed against each other, pressure is generated for the second time (Figure 3d). In fact, the clump model reduces the equilibrium distance between the two elements and subtracts the initial overlap when calculating the relative displacement. In this way, a more complex model can be established. As shown in Figure 3e, the four elements overlap with each other and reach a state of equilibrium. The actual contact is shown in Figure 3f. The element overlapping means that the clump model with a smooth surface can be established.

## 3 | LABORATORY TESTS

### 3.1 | Test process

The schematic diagram of the test device is shown in Figure 4a. In the experiments, two steel pipes with a

diameter of 5 cm and a length of 45 cm were used to represent the adjacent tunnel segments. The distance between the two sections of pipes was set as 2 cm. Four dial gauges were placed above each of the two pipes to monitor the vertical displacements of the pipes. The dial gauges used in the laboratory tests have a maximum range of 20 mm and an accuracy of 0.01 mm, numbered 1–8 from left to right. The spacing between each two dial gauges was 10 cm, and a displacement indicator rod was placed below.

A polyurethane optical fiber with a diameter of 2 mm and a length of about 4 m was glued to the outer wall of pipes using a strong adhesive, and in the directions 0°, 135°, 180°, and 225° (Figure 4b). Optical fiber segments at 0° and 180° were used for quantitative calculations of relative displacements between the pipes, and the optical fiber segments at 135° and 225° were used to correct the results of quantitative calculations.

Two laboratory tests were carried out: the center settlement test, which simulates the relative rotation between adjacent tunnel segments, and the shear test (staggered test), which represents the shear dislocation between adjacent tunnel segments. In the center settlement test (Figure 4c), two pipes are placed on three lifting platforms of the same height. During the test, the height of lifting platforms A1 and A3 remains unchanged. The joint of the two sections of the pipe can be opened and deformed by adjusting the height of lifting platform A2. The central lifting platform A2 is moved downward step by step, and the strain of the optical fiber and data of dial gauges are recorded.

In the shear test (Figure 4d), the left pipe is placed on lifting platforms B1 and B2 of the same height, and the right pipe is placed on lifting platform B3. During the whole testing process, the height of the platforms B1 and B2 remains unchanged, and lifting platform B3 is moved downward to simulate the shear displacement between two pipes.

Both tests were conducted in a constant-temperature laboratory at room temperature of 23.5°C. Therefore, the influence of temperature on the strain value of the optical fiber was not considered. The photos of two laboratory tests on site are shown in Figure 5.

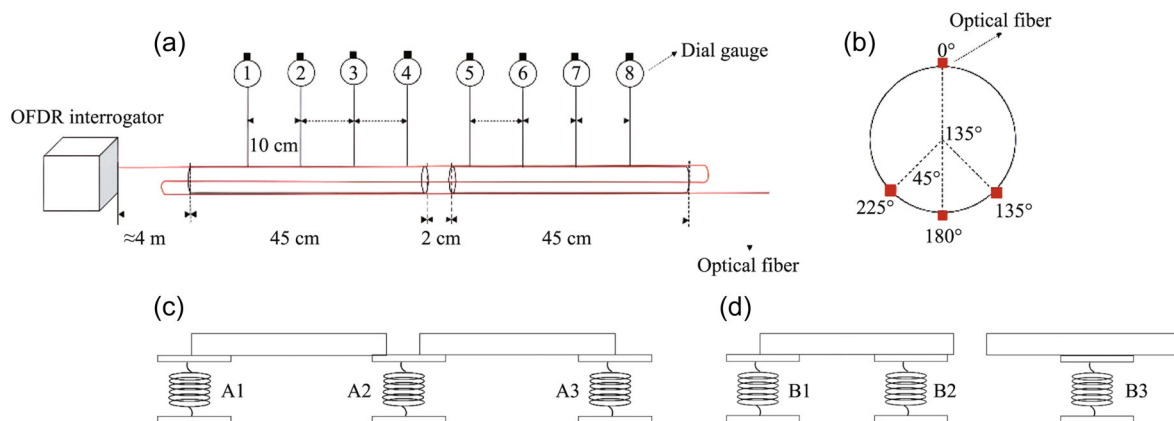


**FIGURE 4** (a) Schematic diagram of the test device, (b) optical fiber's position at the cross section of the pipe, (c) schematic diagram of the center settlement test, and (d) schematic diagram of the shear test.

### 3.2 | Test results and analysis

In the laboratory test, the monitoring position resolution of OFDR was set to 1 cm, which means that the distance between two adjacent optical fiber monitoring data points is 1 cm. The distance between two pipes, respectively, is 2.0003, 2.0009, 2.0012, 2.0028, and 2.0049 cm from Level 1 to Level 5 in the test process for the settlement center. Figure 6 shows the monitored data of the optical fiber at 180° in the center settlement test. With the increase of displacement, the peak value tends to increase gradually. The maximum peak ( $1.4 \times 10^{-3}$ ) occurs in the 5th-level curve. The optical fiber at 180° is only subjected to normal force during the test, so the monitoring results reflect the test process well.

In Figure 4d, it can be seen that in the shear test process, the axial strain detected by the optical fiber at four positions is theoretically the same, so the optical fiber data at 0° position are used for quantitative calculation in this situation.

Figure 7 shows the monitoring data of the optical fiber at 0° during the shearing test. The vertical displacements are 1.14, 1.66, 1.91, 2.17, and 2.36 mm. With the increase of the vertical displacement of the pipeline, the peak value of each curve increases gradually. In all of the curves, the peak value appears at 4.48 m, and another peak value appears between 4.46 and 4.48 m.

The distance between the maximum and secondary microstrain is about 2 cm, so it can be determined that the position between the maximum and secondary microstrain is located at the pipe connection.

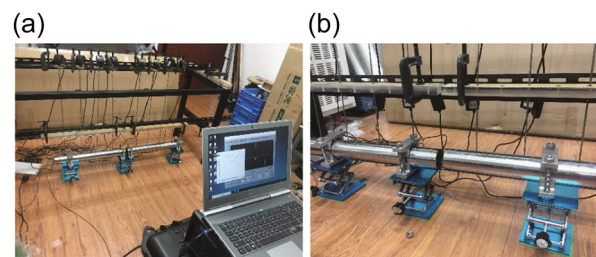


**FIGURE 5** (a) The center settlement test and (b) the shear test.

## 4 | MODELING AND NUMERICAL SIMULATIONS

### 4.1 | Geometrical modeling and material

The geotechnical discrete element numerical simulation software, MatDEM, was developed by Nanjing University independently. Based on the innovative Graphics Processing Unit (GPU) matrix algorithm, the software has the advantages of high computational efficiency, micro- and macro-mechanical parameter conversion, and the ability of secondary development. A three-dimensional discrete

element model of the laboratory test was established in MatDEM.

As shown in Figure 8, the model consists of two parts: tunnels and optical fibers. The simulated tunnel has a radius of 2.5 cm and a length of 45 cm. The relevant research conclusions indicate that if the particle size effect in the discrete element model needs to be eliminated, the ratio of the diameter of the tunnel model to the average particle size needs to be greater than 35 (Bo et al., 2022). Therefore, the diameter of the tunnel model units is set to 1 mm, and the spacing between the two sections of the tunnel is set to 2 cm. A total of four optical fiber models are located at 0°, 135°, 180°, and 225° of the tunnel model cross section (Figure 9). Each optical fiber model consists of a string of particles with a diameter of 2 mm (Figure 10 shows discrete element models of the shear test and the central settlement test). The macroscopic and microscopic mechanical parameters of the optical fiber model and the tunnel model are shown in Tables 1 and 2. All microscopic mechanical parameters of both optical fiber elements and tunnel elements have already been calibrated by automatically training in MatDEM.

For the calculation method proposed in this paper, the following hypotheses have been made:

1. The tunnel does not rotate along the central axis.
2. The displacement of the tunnel occurs only in the Z direction.

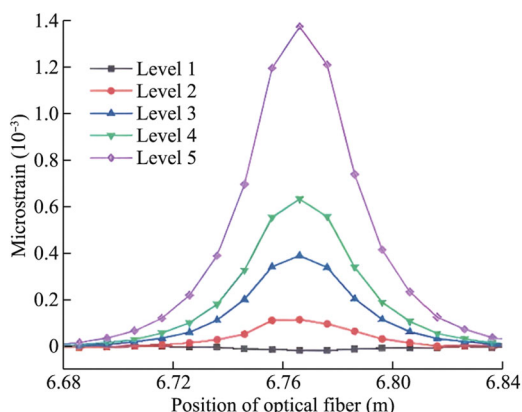


FIGURE 6 Measured strain data of the optical fiber at 180° in the center settlement test.

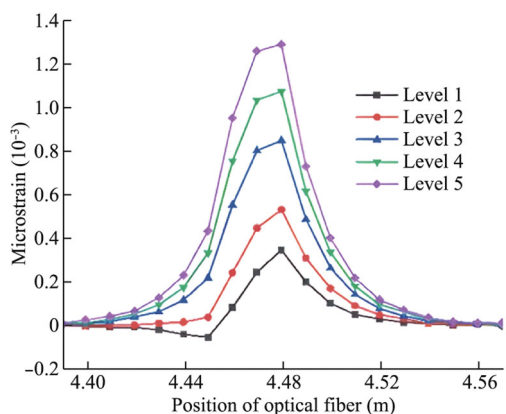


FIGURE 7 Measured strain data of the optical fiber at 0° in the shear test.

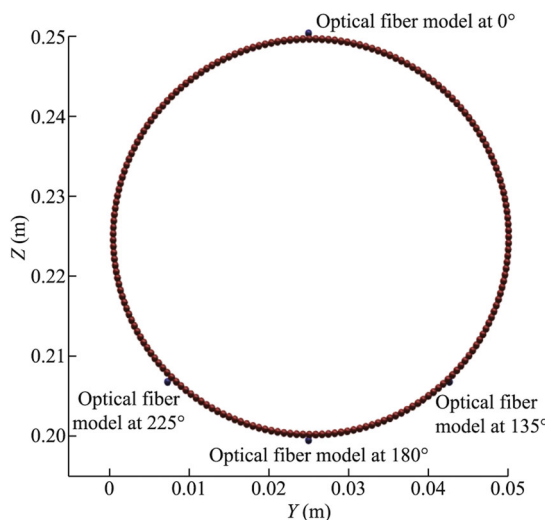


FIGURE 9 A cross section of the model.

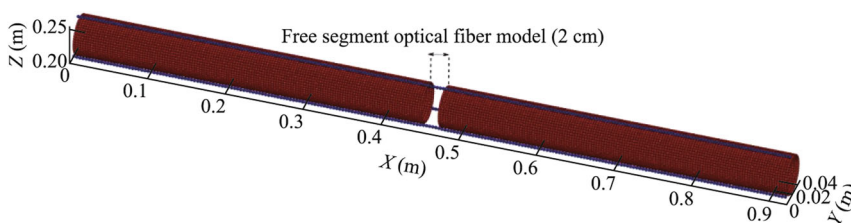
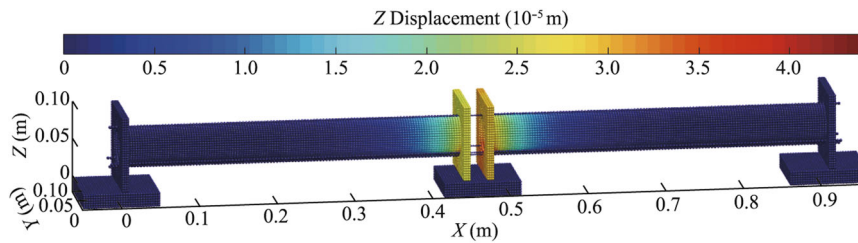


FIGURE 8 Model of tunnels and optical fiber.



**FIGURE 10** Discrete element model of the shear test and the center settlement test.

**TABLE 1** Macroscopic and microscopic mechanical parameters of the optical fiber discrete element model.

Mechanical parameters			Mechanical parameters		
		Value			Value
Macroscopic	Young's modulus (GPa)	60	Microscopic	Normal stiffness (N/m)	$6.74 \times 10^8$
	Poisson's ratio	0.5		Tangential stiffness (N/m)	$1.16 \times 10^8$
	Tensile strength (GPa)	15		Break force (N)	5000
	Compressive strength (GPa)	0.1		Shear resistance (N)	5000
	Coefficient of internal friction	1		Coefficient of friction	0.4
	Density ( $\text{kg/m}^3$ )	50			

**TABLE 2** Macroscopic and microscopic mechanical parameters of the discrete element tunnel model.

Mechanical parameters			Mechanical parameters		
		Value			Value
Macroscopic	Young's modulus (GPa)	206	Microscopic	Normal stiffness (N/m)	$2.31 \times 10^9$
	Poisson's ratio	0.25		Tangential stiffness (N/m)	$3.99 \times 10^8$
	Tensile strength (GPa)	0.4		Break force (N)	5000
	Compressive strength (GPa)	0.1		Shear resistance (N)	2280
	Coefficient of internal friction	1		Coefficient of friction	0.4
	Density ( $\text{kg/m}^3$ )	7850			

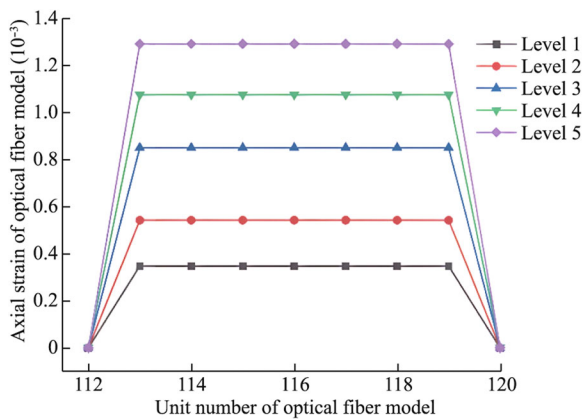


**FIGURE 11** Strain curves of the tunnel center settlement process in the numerical simulation.

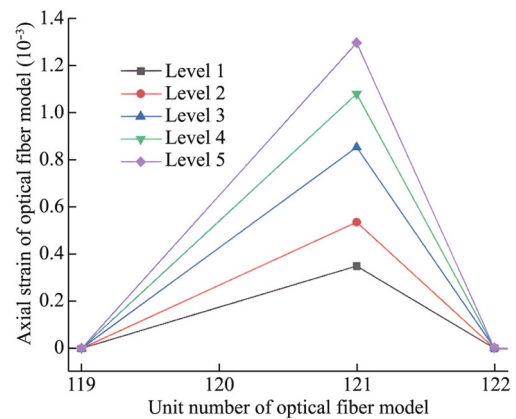


**FIGURE 12** Strain curves of the tunnel shear test process in the numerical simulation.

## 4.2 | Numerical simulations

After the tunnel model and the optical fiber model were established in MatDEM, the physical processes of laboratory tests were numerically simulated in the discrete element model. The strain distribution curves of the optical fiber model obtained from the numerical simulation results are shown in Figures 11 and 12.

Figure 11 shows the strain curves obtained from the optical fiber model at  $180^\circ$  in the numerical simulation of the central settlement process. It appears that the peak value of each curve exists from the 113th to the 119th unit. The unit radius of the optical fiber model is 0.2 cm, so the distance between the 113th and the 119th unit is 2.4 cm. It can be judged that the free segment of optical fiber model with the length of 2 cm is between

the 113th unit and the 119th unit. Also, all units of the free segment of the optical fiber model reach the same peak strain value, indicating that the normal springs among these units are fully stretched in the numerical simulation process. The strain transfer range, namely, the distance from the edge of the pipe to the point where the strain of the optical fiber can reach the maximum model at  $180^\circ$  near the strain peak, is within 0.4 cm.

Figure 12 shows the strain curves obtained from the optical fiber model at  $0^\circ$  in the numerical simulation of the tunnel shear process. The horizontal axis is the unit number of the optical fiber model, and the vertical axis is the axial strain of the optical fiber model. The peak of each curve appears at the position of unit 121. At the same time, it can be found that the strain value fluctuates considerably between the 119th unit and the 122nd unit. The unit radius of the optical fiber model is 0.2 cm, so the distance between the 119th unit and the 122nd unit is 1.2 cm. Therefore, it can be judged that the units between the 119th unit and the 122nd unit belong to the free segment of the optical fiber model with a length of 2 cm. Besides, it can be found that the strain transfer range is within 0.8 cm near the strain peak.

## 5 | QUANTITATIVE CALCULATION

### 5.1 | Quantitative calculation principle of the center settlement test

As shown in Figure 13, when the two sections of the tunnel rotate along the fixed ends, respectively, the opening  $C$  of the discontinuous ends of the two sections of the tunnel is calculated as follows:

$$C = a + \Delta a, \quad (6)$$

$$\varepsilon = \Delta a/a, \quad (7)$$

where  $a$  denotes the original opening and  $\varepsilon$  denotes the axial strain of the optical fiber at the opening.

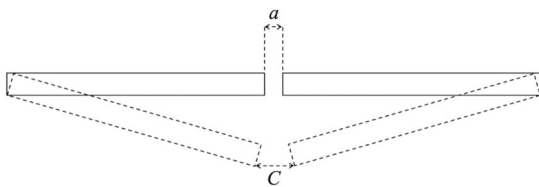


FIGURE 13 Quantitative calculation principle of the center settlement test.

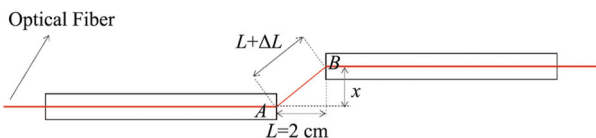


FIGURE 14 Quantitative calculation principle of the shear test.

### 5.2 | Quantitative calculation principle of the shear test

When vertical shear deformation occurs in the tunnel, the increased length of the free segment fiber being stretched is  $\Delta L$ , and the distance between  $A$  and  $B$  is  $(L + \Delta L)$ . The vertical shear deformation of the tunnel can be obtained by transferring the peak strain to the value  $\Delta L$ . The quantitative calculation principle of the shear test is shown in Figure 14.

The derivation process of the calculation formula is as follows:

$$\varepsilon = \Delta L \div L, \quad (8)$$

$$x = \sqrt{(L + \Delta L)^2 - L^2}, \quad (9)$$

Therefore:

$$x = \sqrt{L^2 \times (1 + \varepsilon)^2 - L^2}, \quad (10)$$

where  $\Delta L$  is the variation of length of the fiber;  $L$  is the original length of the optical fiber; and  $x$  is the shear deformation of the tunnel.

### 5.3 | Quantitative calculation results

Figure 15 shows the quantitative calculation results of the shear test. The figure compares the measured data of dial indicators, the vertical displacement of the pipe calculated from the measured data of the optical fiber, and the calculation results of the numerical model. It can be found that in each loading stage, the measured data of dial indicators are the largest, followed by the calculation results of the numerical model, and the vertical displacement of the pipe calculated from the measured data of the optical fiber is the smallest. During the shear test, the vertical displacement of the pipe is no more than 2.4 mm, which is quite small. Therefore, the distributed optical fiber may not be able to perceive the displacement changes of the pipe precisely. For the discrete element numerical model, six parameters of rock and soil mass (namely, Young's modulus, Poisson's ratio, tensile strength, compressive strength, internal friction coefficient, and density)

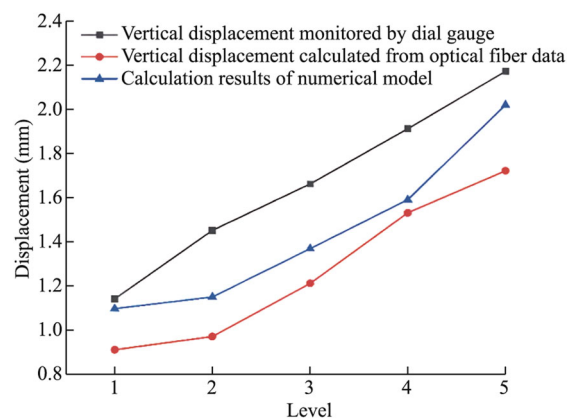
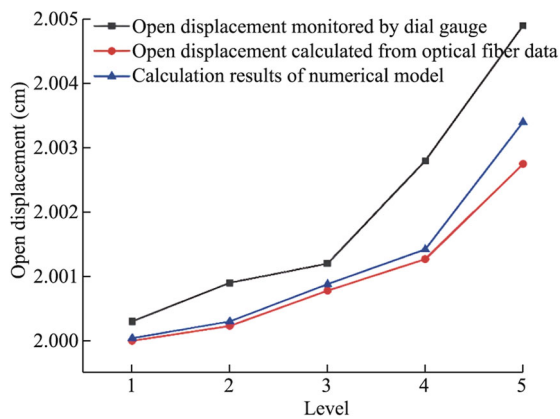


FIGURE 15 Quantitative calculation results of the shear test.



**FIGURE 16** Quantitative calculation results of the center settlement test.

need to be input during the modeling. However, steel pipe and polyurethane optical fiber are not traditional geotechnical materials, so it is difficult to determine the parameters of these two materials, because of which the calculation results of the numerical model are less than the measured data of dial indicators. Figure 16 shows the quantitative calculation results of the center settlement test. It shows similar information as the shear test.

## 6 | CONCLUSIONS

In this study, a quantitative calculation method for the displacement of the shear process and the central settlement process at the joint of the tunnel was proposed. A laboratory test was designed under two conditions, and a discrete element numerical simulation was carried out for the test process. The conclusions are as follows:

1. OFDR distributed optical fiber sensing technology has the characteristics of high resolution. Accordingly, it is feasible for use in the tunnel deformation monitoring process, and it can be used to conduct quantitative monitoring of the displacement at the tunnel connection.
2. An elastic clump model based on the particle DEM was proposed in this study. A 3-dimensional tunnel model was established.
3. The optical fiber, which is formed by atypical geotechnical materials, was applied in discrete element modeling and numerical simulation. The numerical simulation results could accurately reflect the strain distribution in the numerical simulation process.
4. The quantitative calculation method for the shear test and the central settlement test is feasible.
5. The length of the deformation zone around the joint is around 0.16 m in both the tests.
6. For the optical fiber crossing the joint, the strain will reach the peak within 0.4 cm in the central settlement process, but it takes longer to reach its maximum in the shear test based on DEM simulation.

In the shear test and the center settlement test, the displacement calculated quantitatively is slightly less than the measured displacement of the dial gauge. Therefore, both the accuracy of OFDR distributed optical fiber sensing and the discrete element simulation of the deformation at the joint of the tunnel need to be improved.

## ACKNOWLEDGMENTS

The authors gratefully acknowledge financial support from the below-mentioned agencies. This work was financially supported by the National Natural Science Foundation of China (Grant Nos. 42222707 and 41977218) and the 2020 Open-end Research Foundation of the State Key Laboratory for Geomechanics and Deep Underground Engineering (SKLGDUEK2117).

## CONFLICT OF INTEREST STATEMENT

The authors declare no conflict of interest.

## DATA AVAILABILITY STATEMENT

The data that support the findings of this study are available on request from the corresponding author. The data are not publicly available due to privacy and ethical restrictions.

## ORCID

Maoyi Mao  <http://orcid.org/0009-0002-0603-7552>

## REFERENCES

- Bakker KJ, De Boer F, Admiraal JBM, Van Jaarsveld EP. Monitoring pilot projects using bored tunnelling: the Second Heinenoord Tunnel and the Botlek Rail Tunnel. *Tunnel Undergr Space Technol.* 1999;14(2):121-129. doi:10.1016/S0886-7798(99)00025-5
- Bo YJ, Wang HN, Jiang MJ, Che N. Particle size effect of tunnel mechanical state in discrete element simulation. *Chin J Undergr Space Eng.* 2022;18(5):1471-1480.
- Caratelli A, Meda A, Rinaldi Z, Romualdi P. Structural behaviour of precast tunnel segments in fiber reinforced concrete. *Tunnel Undergr Space Technol.* 2011;26(2):284-291. doi:10.1016/j.tust.2010.10.003
- Cheng WC, Ni JC. Feasibility study of applying SOFO optical fiber sensor to segment of shield tunnel. *Tunnel Undergr Space Technol.* 2009;24(3):331-349. doi:10.1016/j.tust.2008.08.005
- Fajkus M, Nedoma J, Mec P, Hrubesova E, Martinek R, Vasinek V. Analysis of the highway tunnels monitoring using an optical fiber implemented into primary lining. *J Electr Eng.* 2017;68(5):364-370. doi:10.1515/jee-2017-0068
- Gómez J, Casas JR, Villalba S. Structural health monitoring with distributed optical fiber sensors of tunnel lining affected by nearby construction activity. *Autom Constr.* 2020;117:103261. doi:10.1016/j.autcon.2020.103261
- Guan K, Zhu W, Liu X, Wei J. Finite strain analysis of squeezing response in an elastic-brittle-plastic weak rocks considering the influence of axial stress. *Tunnel Undergr Space Technol.* 2020;97:103254. doi:10.1016/j.tust.2019.103254
- Gue CY, Wilcock M, Alhaddad MM, Elshafie MZEB, Soga K, Mair RJ. The monitoring of an existing cast iron tunnel with distributed fibre optic sensing (DFOS). *J Civil Struct Health Monit.* 2015;5:573-586. doi:10.1007/s13349-015-0109-8
- Hashimoto T, Ye G, Nagaya J, Konda T, Ma X. Study on earth pressure acting upon shield tunnel lining in clayey and sandy grounds based on field monitoring. *Geotechnical Aspects of Underground Construction in Soft Ground: Proceedings of the 6th International Symposium (IS-Shanghai 2008)*. CRC Press; 2008:307.
- Huang H, Li Q, Zhang D. Deep learning based image recognition for crack and leakage defects of metro shield tunnel. *Tunnel Undergr Space Technol.* 2018;77:166-176. doi:10.1016/j.tust.2018.04.002

- Jallow A, Ou CY, Lim A. Three-dimensional numerical study of long-term settlement induced in shield tunneling. *Tunnel Undergr Space Technol.* 2019;88:221-236. doi:10.1016/j.tust.2019.02.021
- Juárez-Luna G, Tenorio-Montero E. Formulation of a thick beam-column element with embedded discontinues for modelling hinges in simple and double-lined tunnels. *Tunnel Undergr Space Technol.* 2019;93:103091. doi:10.1016/j.tust.2019.103091
- Katebi H, Rezaei AH, Hajjalilue-Bonab M, Tarifard A. Assessment the influence of ground stratification, tunnel and surface buildings specifications on shield tunnel lining loads (by FEM). *Tunnel Undergr Space Technol.* 2015;49:67-78. doi:10.1016/j.tust.2015.04.004
- Kavvasdas MJ. Monitoring ground deformation in tunnelling: current practice in transportation tunnels. *Eng Geol.* 2005;79(1-2):93-113. doi:10.1016/j.enggeo.2004.10.011
- Kawakami H. Evaluation of deformation of tunnel structure due to Izu-Oshima-Kinkai earthquake of 1978. *Earthquake Eng Struct Dyn.* 1984;12(3):369-383. doi:10.1002/eqe.4290120306
- Koyama Y. Present status and technology of shield tunneling method in Japan. *Tunnel Undergr Space Technol.* 2003;18(2-3):145-159. doi:10.1016/S0886-7798(03)00040-3
- Lee YJ, Bassett RH. A model test and numerical investigation on the shear deformation patterns of deep wall-soil-tunnel interaction. *Can Geotech J.* 2006;43(12):1306-1323. doi:10.1139/t06-088
- Li S, Li P, Zhang M. Analysis of additional stress for a curved shield tunnel. *Tunnel Undergr Space Technol.* 2021;107:103675. doi:10.1016/j.tust.2020.103675
- Liu C, Pollard DD, Shi B. Analytical solutions and numerical tests of elastic and failure behaviors of close-packed lattice for brittle rocks and crystals. *J Geophys Res Solid Earth.* 2013;118(1):71-82. doi:10.1029/2012JB009615
- Ma GM, Zhou HY, Li YB, et al. High-resolution temperature distribution measurement of GIL spacer based on OFDR and ultraweak FBGs. *IEEE Trans Instrum Meas.* 2020;69(6):3866-3873. doi:10.1109/TIM.2019.2937408
- Mohamad H, Soga K, Bennett PJ, Mair RJ, Lim CS. Monitoring twin tunnel interaction using distributed optical fiber strain measurements. *J Geotech Geoenviron Eng.* 2012;138(8):957-967. doi:10.1061/(ASCE)GT.1943-5606.0000656
- Monsberger CM, Lienhart W. Distributed fiber optic shape sensing along shotcrete tunnel linings: methodology, field applications, and monitoring results. *J Civil Struct Health Monitor.* 2021;11(2):337-350. doi:10.1007/s13349-020-00455-8
- Moussaei N, Sharifzadeh M, Sahriar K, Khosravi MH. A new classification of failure mechanisms at tunnels in stratified rock masses through physical and numerical modeling. *Tunnel Undergr Space Technol.* 2019;91:103017. doi:10.1016/j.tust.2019.103017
- Nomoto T, Imamura S, Hagiwara T, Kusakabe O, Fujii N. Shield tunnel construction in centrifuge. *J Geotech Geoenviron Eng.* 1999;125(4):289-300. doi:10.1061/(ASCE)1090-0241(1999)125:4(289)
- Sun H, Liu S, Zhong R, Du L. Cross-section deformation analysis and visualization of shield tunnel based on mobile tunnel monitoring system. *Sensors.* 2020;20(4):1006. doi:10.3390/s20041006
- Wang J, Liu H, Liu H, Zou Y. Centrifuge model study on the seismic responses of shield tunnel. *Tunnel Undergr Space Technol.* 2019;92:103036. doi:10.1016/j.tust.2019.103036
- Wang X, Shi B, Wei G, Chen SE, Zhu H, Wang T. Monitoring the behavior of segment joints in a shield tunnel using distributed fiber optic sensors. *Struct Control Health Monitor.* 2018;25(1):e2056. doi:10.1002/stc.2056
- Wei G, Yu G, Hong W. Study on calculation of shield tunnel shearing dislocation platform deformation due to adjacent ground stacked

load. *J Cent South Univ (Sci Technol).* 2018;49:1775-1783. doi:10.11817/j.issn.1672-7207.2018.07.026

- Xiong X, Song G, Chen H, Zhou Q, He Z. Principle and realization method of tunnel deformation detection based on image recognition and data transmission technology. *Eng Sci.* 2010;8(4):23-25.
- Zhang X, Broere W. Monitoring seasonal deformation behavior of an immersed tunnel with distributed optical fiber sensors. *Measurement.* 2023;219:113268. doi:10.1016/j.measurement.2023.113268
- Zhao S, Zhang DM, Huang HW. Deep learning-based image instance segmentation for moisture marks of shield tunnel lining. *Tunnel Undergr Space Technol.* 2020;95:103156. doi:10.1016/j.tust.2019.103156

## AUTHOR BIOGRAPHY



**Chun Liu** is a professor at Nanjing University. He graduated from Nanjing University in 2012 and won the Jiangsu Province Excellent Doctoral Thesis Award. After the postdoctoral research at Stanford University, he joined

Nanjing University in 2014. His research interest lies in the discrete element method, software development, and engineering applications. He has hosted or been part of 10 National Natural Science Foundation projects, including the National Excellent Youth Science Foundation Project. He has published about 100 academic papers, with over 1700 citations. He has applied for and obtained over 20 national invention patents, two PCT international patents. Since 2011, he independently developed the high-performance discrete element software MatDEM, for which he received the “China Digital Simulation Independent Software Innovation Award” and the Silver Award at the Geneva International Invention Exhibition. He won the First Prize of the Natural Science Award of the Ministry of Education and the “Qian Qihu Award” in 2022, and the Jiangsu Patent Silver Award in 2023. He is currently the Vice Chairman of the Chinese National Group of the International Society for Rock Mechanics and Rock Engineering, the Deputy Secretary General of the Chinese Society of Rock Mechanics and Engineering, and so on.

**How to cite this article:** Mao M, Yang X, Liu C, Zhao T, Liu H. Deformation monitoring at shield tunnel joints: laboratory test and discrete element simulation. *Deep Undergr Sci Eng.* 2024;1-9. doi:10.1002/dug2.12092